Platinum Nanoparticle Ensemble-on-Graphene Hybrid Nanosheet: One-Pot, Rapid Synthesis, and Used as New Electrode Material for Electrochemical Sensing

Shaojun Guo,[†] Dan Wen,[†] Yueming Zhai, Shaojun Dong,* and Erkang Wang*

State Key Laboratory of Electroanalytical Chemistry, Changchun Institute of Applied Chemistry, Chinese Academy of Sciences, Changchun 130022, Jilin, China, and Graduate School of the Chinese Academy of Sciences, Beijing, 100039, P. R. China. [†]These authors contributed equally to this work.

ABSTRACT The development of nanoscience and nanotechnology has inspired scientists to continuously explore new electrode materials for constructing an enhanced electrochemical platform for sensing. In this article, we proposed a new Pt nanoparticle (NP) ensemble-on-graphene hybrid nanosheet (PNEGHNs), a new electrode material, which was rapidly prepared through a one-step microwave-assisted heating procedure. The advantages of PNEGHNs modified glassy carbon electrode (GCE) (PNEGHNs/GCE) are illustrated from comparison with the graphenes (GNs) modified GCE for electrocatalytic and sensing applications. The electrocatalytic activities toward several organic and inorganic electroactive compounds at the PNEGHNs/GCE were investigated, all of which show a remarkable increase in electrochemical performance relative to GNs/GCE. Hydrogen peroxide (H_2O_2) and trinitrotoluene (TNT) were used as two representative analytes to demonstrate the sensing performance of PNEGHNs. It is found that PNEGHNs modified GCE shows a wide linear range and low detection limit for H_2O_2 and TNT detection. Therefore, PNEGHNs may be an attractive robust and advanced hybrid electrode material with great promise for electrochemical sensors and biosensors design.

KEYWORDS: graphene · Pt nanoparticle · hybrid nanomateirals · sensor · electrocatalysis

Nanoelectroanalytical chemistry is a rising interdisciplinary field, which combines characteristics of electrochemistry (*e.g.*, high sensitivity, small dimension, rapid detection, low cost, and compatibility with microfabrication technology) with unique properties of nanomaterials (*e.g.*, electronic, optical, magnetic, mechanical, and catalytic) to become one of the most exciting topics.[1,2] Particularly, carbon nanomaterials including carbon nanotubes (CNTs),[3−11] carbon nanofibers,[12−14] highly ordered mesoporous carbon (OMCs),[15−17] and carbon nanohorns,[18−20] *etc.* have been widely used in electroanalytical investigations and have enormous potentials for constructing electrochemical sensing platforms with high sensitivity to detect different target molecules, because of their chemical inertness, relatively wide potential window, low background current, and suitability for different types of analysis. For instance, many studies have revealed that CNTs have good electrochemical behavior toward cytochrome *c*,[3] ascorbic acid,[4,7] β-nicotinamide adenine dinucleotide (NADH),[4] dopamine (DA),[5,8,9] arsenite,[6,10] and uric acid,[11] *etc.*, since they are conductive, biocompatible, easily functionalized, and possess very large surface areas. And, OMCs have been used as enhanced components for constructing electrochemical sensing platform for L-cysteine, NADH, ethanol, and glucose, *etc.*, owing to the extremely high surface area, defined pore size, high thermal stability, and flexible framework composition.[15−17] Despite such advanced electroanalytical capability of theses carbon nanomaterials, there still has been significant interest in the development of new carbon nanomaterial to accelerate the development of electroanalycial chemistry.[18−20]

Graphene nanosheet (GN), a "rising star" material, has received considerable interest due to its high surface areas (calculated value, 2630 m^2/g), low cost, and high conductivity (10^3-10^4 S/m).[21−23] It is flexible yet stronger than diamond[24] and has a huge electrical mobility approaching 200 000 $cm^2 V^{-1} s^{-1}$ for a free sheet for both electrons and holes.[25] These unique characteristics hold great promise for potential applications in many technological fields such as nanoelectronics,[26−28] nanophotonics,[29] nanocomposites,[30,31] catalysis,[32] batteries,[33] supercapacitors[34] and dye-sensitized

*Address correspondence to dongsj@ciac.jl.cn, ekwang@ciac.jl.cn.

Received for review April 22, 2010 and accepted June 16, 2010.

Published online June 22, 2010. 10.1021/nn100852h

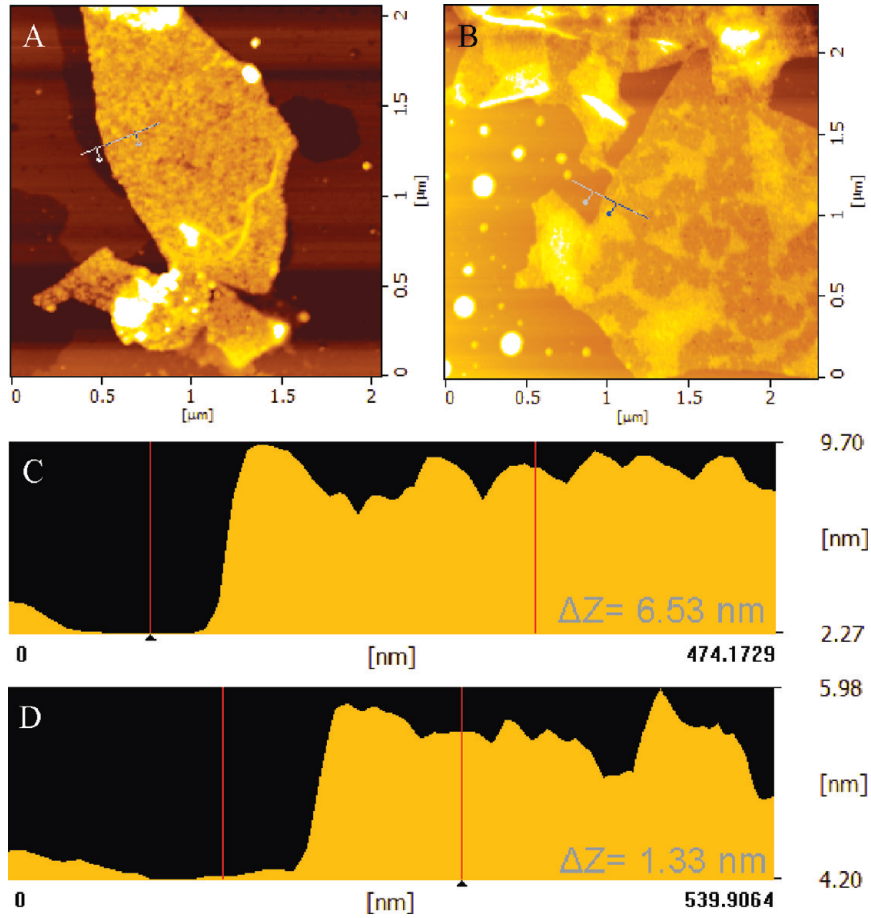

Figure 1. AFM images of PNEGHNs (A) and PMAA-functionalized GN (B). (C) The cross section identified by the line in Figure 1A shows the height of individual PNEGHNs; (D) The cross section identified by the line in Figure 1B shows the height of GNs.

solar cell.[35] However, to the best of our knowledge, there have been a few studies on its electroanalytical applications for electrocatalysis.[36−40] For instance, Li's group[36] reported the basic electrochemical properties of reduced GN film-modified GCE, which exhibited enhanced electrocatalytic activity for some electroactive species. Dong *et al.*[37] demonstrated an advanced electrochemical sensing and biosensing platform prepared through casting GNs on the surface of GCE, which shows much higher electrocatalytic activity toward NADH, DA, and other biological molecules than that of graphite. Although GNs show obvious advantages for analytical applications, it is very necessary to explore new GNs-based functional materials with much higher electroanalytical ability.

The clever combination of different nanoscaled inorganic nanomaterials, leading to the development of a multifunctional nanoassembly system with enhanced optical, electronic, and catalytic properties, may open a new avenue for utilizing GN-based hybrid nanomaterials as enhanced elements for constructing electrochemical sensing platform with high performance. This is because hybrid nanomaterials (*e.g.*, a carbon/Au-NP hybrid system) could provide larger electrochemically active surface areas for the adsorption of biomolecules and effectively accelerate the electron transfer between electrode and detection molecules, which could lead to a more rapid and sensitive current response. At present, although several groups have developed some strategies for obtaining GN/Pt hybrid nanostructures with enhanced performance for fuel-cell reactions,[41−45] a one-step route for synthesizing high-quality GN/Pt NPs hybrids as enhanced platform for electroanalytical applications is rarely a concern.[46] In this article, we for the first time reported a one-step, microwave-assisted route for rapidly synthesizing Pt NP ensemble-on-graphene hybrid nanosheets (PNEGHNs), which have several important benefits. (1) Pt NPs on GNs with high conductivity have small size (~2.6 nm) and good size distribution; (2) Pt NPs could form a uniform distribution on the surface of GNs; (3) Pt NPs have a controllable high-metal-loading level on GNs; all of which are important for optimizing a Pt NP's performance and facilitating the electroanalytical applications of the above hybrids. Inspired by this, the characterization and electroanalytical application of PNEGHNs modified GCE, a novel hybrid electrode system, for the preparation of electrochemical sensing platform are demonstrated. Different kinds of important electroactive compounds (*e.g.*, probe molecule (potassium ferricyanide), hydro-

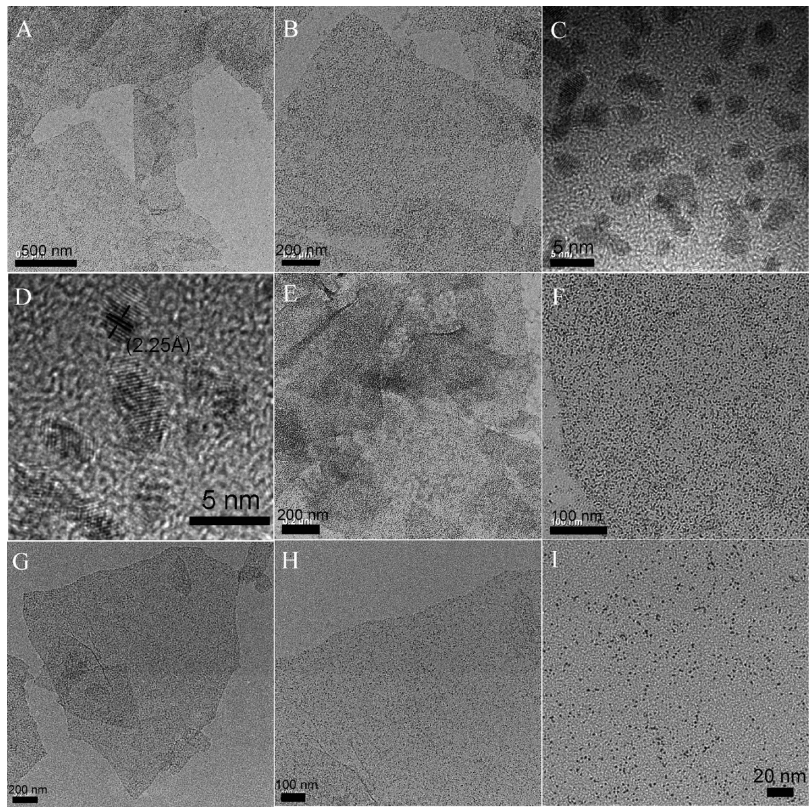

Figure 2. TEM (A−C) images of PNEGHNs (GPt2) at different magnifications. HRTEM of Pt NPs (D). TEM (E, F) images of PNEGHNs with relative high density of Pt NPs (GPt3) at different magnifications. TEM (G−I) images of PNEGHNs with relative low density of Pt NPs (GPt1) at different magnifications.

gen peroxide, neurotransmitters (DA), acetaminophen (APAP), and TNT) were employed to study their electrochemical responses at the PNEGHNs/GCE. It is interestingly found that PNEGHNs/GCE shows more favorable electron transfer kinetics and much enhanced electrochemical reactivity than GNs/GCE, which provide a kind of more robust and advanced hybrid electrode material with great promise for electrochemical sensors and biosensors design.

RESULTS AND DISCUSSION

Characterization of PNEGHNs. Microwave heating has been proven to be a promising method for rapid volumetric heating, which could result in higher reaction rates and selectivities, reduction in reaction times often by orders of magnitude, and increasing yields of products compared to conventional heating methods.[47] PNEGHNs were facilely obtained through heating a water/ethylene glycol (EG) mixture containing graphene oxide, Pt precursor and poly(methacrylic acid sodium salt) (PMAA) under the microwave-assisted heating method. Herein, EG was used as a reducing agent for the effective reduction of both GO and Pt precursor. Dai *et al.*[48] showed that an effective solvothermal reduction method could effectively decrease the number of defects and the oxygen content, thus increase the size of sp^2 domains in GNs relative to traditional hydrazine reduction method.[21] Therefore, it is expected that GN obtained by the present strategy has low defect due to the high reduction rate provided by microwave microenvironment. Moreover, PMAA plays a dual role in obtaining PNEGHNs. That is, PMAA cannot only stabilize GNs due to the strong hydrophobic interaction between PMAA and GNs, but also they can act as a linker or protecting agent for obtaining small Pt NPs. Figure 1A shows the typical atomic force microscopic (AFM) image of PNEGHNs (GPt2). It is observed that the mica substrate is covered with several typical nanosheets, which have a rougher surface than that of the PMMA-functionalized GNs (Figure 1B). The thickness of PNEGHNs and GNs is about 6.5 nm (Figure 1C) and 1.3 nm (Figure 1D), respectively. The morphology and structure of PNEGHNs were further examined by transmission electron microscopy (TEM) and high-resolution TEM (HRTEM). Figure 2A−C shows the typical TEM images of the product at different magnifications. Low-magnification TEM images (Figure 2A,B) show that many small Pt NPs with good size distribution are uniformly distributed on the graphene. The absence of isolated Pt NPs in the product reveal that the link between GN and Pt NPs is strong. The magnified image (Figure 2C) shows that these Pt NPs have the size of about 2.6 nm. The HRTEM of Pt NPs is shown in Figure 2D. The *d*-spacings of adjacent fringe for Pt is 2.25 Å′, corresponding to the {111} plane of face-centered cubic (fcc) Pt, which indicates that Pt NPs have been fac-

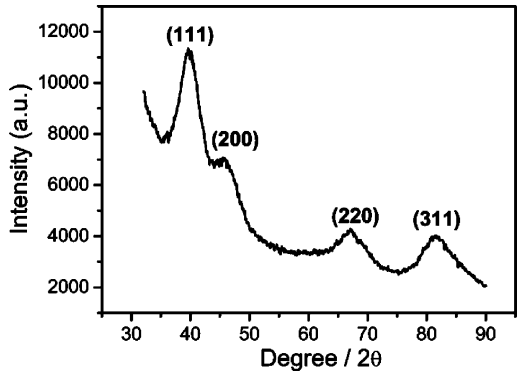

Figure 3. XRD pattern of PNEGHNs.

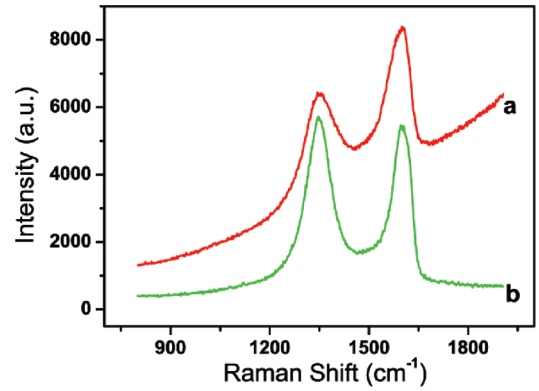

Figure 5. Raman spectroscopy of GO (a) and PNEGHNs (b).

ilely obtained. Interestingly, the density of Pt NPs on GNs could be easily controlled *via* simply changing the reaction parameters. For instance, PNEGHNs with higher density of Pt NPs could be obtained when 2 mL of Pt precursor was added into the mixture instead of 1 mL of Pt precursor, as shown in Figure 2E, F (GPt3). Whereas the amount of Pt precursor was decreased to 0.5 mL, the density of Pt NPs supported on GNs could be further reduced (Figure 2G−I, GPt1). In addition, compared with the previous reports for GNs/Pt hybrids,[36−40] in which the obtained Pt NPs have a relatively wide size range and nonuniform distribution on the surface of graphene, the present microwave-assisted strategy provides a more obvious advantage for obtaining high-quality GNs/Pt hybrids with Pt NPs of controllable density, small size, and uniform distribution. This is because that microwave system can provide a good microenvironment for Pt rapid nucleus, which is important for obtaining small Pt NPs. As introduced above, PMAA has also played an important role for obtaining uniform Pt NPs and acted as an effective linker for constructing PNEGHNs with controllable density of Pt NPs.

The formation of PNEGHNs was further characterized by X-ray diffraction (XRD) (Figure 3), X-ray photoelectron spectroscopy (XPS) (Figure 4), and Raman spectroscopy (Figure 5). The XRD pattern of PNEGHNs shows obvious peaks corresponding to the (111), (200), (220), and (311) diffraction peaks of fcc Pt (JCPDS: 87-0647), indicating that Pt exists in the form of crystalline state. XPS patterns of the resulting PNEGHNs show significant Pt4f signals corresponding to the binding energy of Pt (Figure 4A) and significant C signal corresponding to the binding energy of GN (Figure 4B), further supporting the conclusion that Pt NPs have been effectively assembled on the surface of GNs. The reduction of GO to GNs could be further characterized by XPS. The XPS spectrum of GO (Figure 4C) indicates the presence of 2 main types of carbon bonds: C−C (284.6 eV) and C−O (286.7 eV), etc.[49,50] After its reduction (Figure 4B), the peaks associated with C−C (284.6 eV) became predominant, while the peaks related to the oxidized carbon species were greatly weakened. The peak at 288.7 eV is from COO^- of PMAA. These results further indicate that GO has been well deoxygenated to form GNs, which is very important for improving its conductivity. Raman spectroscopy is a useful nondestructive tool to characterize carbonaceous materials, particularly for distinguishing ordered and disordered carbon structures. G band is usually assigned to the E_{2g} phonon of C sp^2 atoms, while D band is a breathing mode of κ-point phonons of A_{1g} symmetry. Figure 5 shows the Raman spectroscopy of GO (a) and PNEGHNs (b). The frequencies of the G and D bands in the PNEGHNs are similar to those observed in the GO. But PNEGHNs have an increased D/G intensity ratio relative to GO. This change suggests a decrease in the size of the in-plane sp^2 domains and a partially ordered crystal structure of GNs.[21−23] Therefore, the data from HRTEM, XPS, and Raman spectroscopy clearly demonstrate that GO were successfully reduced to GNs.

Electrochemical Activity and Sensing of PNEGHNs. $Fe(CN)_6^{3-/4-}$ redox probe was selected to study the electrochemical properties of PNEGHNs. Cyclic voltam-

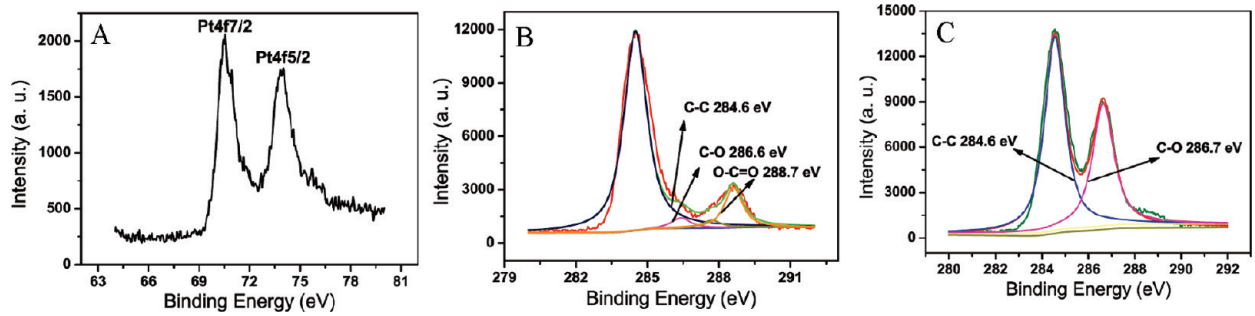

Figure 4. XPS spectroscopy (A, B) of PNEGHNs: (A) Pt 4f; (B) C1s. The deconvolution of C1s spectra of PNEGHNs (B) and GO (C).

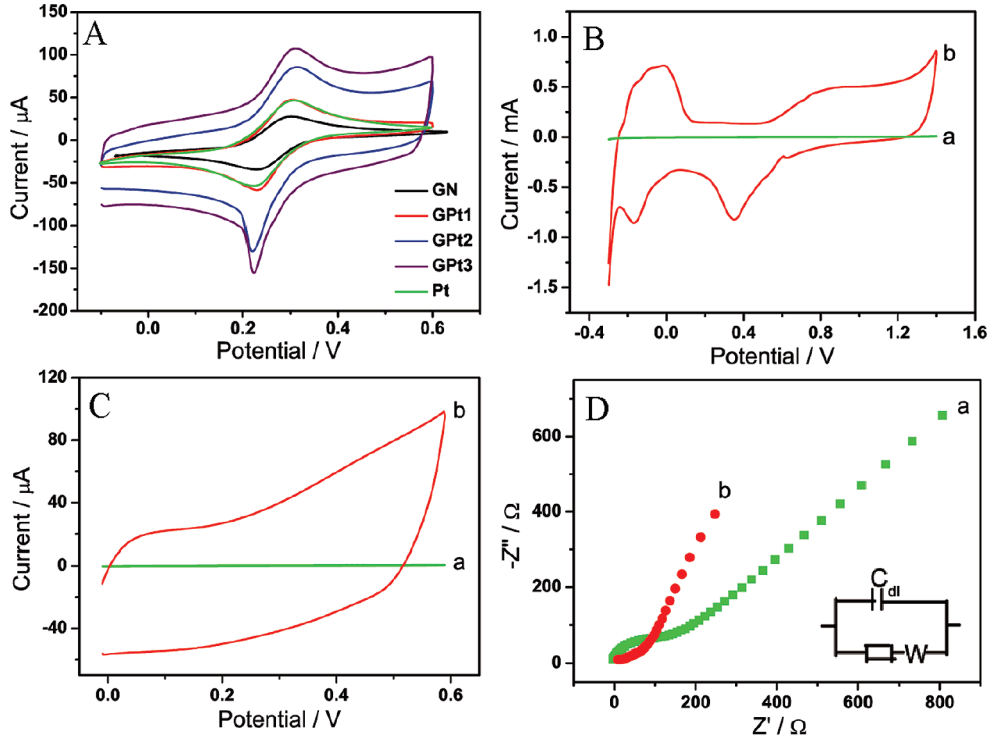

Figure 6. (A) CVs of GNs/GCE (a), Pt NPs/GCE (b), and PNEGHNs/GCE with different densities of Pt NPs (c−e) in 0.1 M KCl solution containing 5.0 mM $K_3Fe(CN)_6^{3-}$ at the scan rate of 50 mV/s. (B) CVs of GNs/GCE (a) and PNEGHNs/GCE (b) in a 0.5 M H_2SO_4 solution at the scan rate of 50 mV/s. (C) CVs of GNs/GCE (a) and PNEGHNs/GCE (b) in a PBS (pH 7.0) at the scan rate of 50 mV/s. (D) EIS plots of GNs/GCE (a) and PNEGHNs/GCE (b) in 0.1 M KCl solution containing 5.0 mM $Fe(CN)_6^{3-/4-}$.

mograms (CVs) of 5.0 mM $K_3Fe(CN)_6^{3-}$ in 0.5 M KCl solution on GNs/GCE, Pt NPs (their TEM image is shown in Supporting Information, Figure S1)/GCE and PNEGHNs/GCE with different densities of Pt NPs are shown in Figure 6A. The quasi-reversible one-electron redox behavior of ferricyanide ions was observed on the above modified electrodes. However, after GCE was modified with PNEGHNs (*e.g.*, blue line), the peak current of $Fe(CN)_6^{3-/4-}$ increased relative to that modified with GNs, indicating that the introduction of the PNEGHNs played an important role in the increase of the electroactive surface area and providing the conducting bridges for the electron-transfer of $Fe(CN)_6^{3-/4-}$. Figure 6A also shows the effect of Pt loading amounts on the CVs of $Fe(CN)_6^{3-}$. It is observed that increasing Pt loading (from GPt1 to GPt3) increased the redox peak currents (note that all three samples have the same amount of GNs). These effects are attributed to increased surface area and surface roughness due to the increased amount of Pt NPs. Note that GPt3 only exhibited a slightly enhanced current as compared to GPt2. Thus, considering the high cost of Pt, we employed GPt2 as an enhanced material for the following electrochemical sensing. In addition, PNEGHNs/GCE (blue line) exhibited a higher electrochemical activity than Pt NPs/GCE (green line) under the condition of the same amount of Pt loading, indicating that GNs play an important role in enhancing Pt activity, which is in good accordance with a previous report.[21] Figure 6B depicts CVs of GNs (a) and PNEGHNs (b) in 0.5 M H_2SO_4 acquired at a scan rate of 50 mV/s. Hydrogen adsorption/desorption and oxide formation/reduction regions of Pt are obviously observed in PNEGHNs, indicating that Pt NPs have been effectively loaded on the GNs. In view of the electrochemical response being highly sensitive to the physicochemical properties of the surface, background CVs were used to examine the PNEGHNs. Figure 6C shows CVs of GNs and PNEGHNs in 0.1 M phosphate buffer solution (PBS, pH 7.0) acquired at a scan rate of 50 mV/s. It is observed that the double layer capacitance at the PNEGHNs is much higher than that of GNs, which means PNEGHNs have a much higher electrochemical active area, thus are a promising material for electrochemical applications. Electrochemical impedance spectroscopy (EIS) is also an efficient tool for studying the interface properties of surface-modified electrodes. The charge-transfer resistance (R_{ct}) at the electrode surface is equal to the semicircle diameter of EIS and can be used to describe the interface properties of the electrode. Thus, the capability of electron transfer of different electrodes was further investigated by EIS experiments. Figure 6D indicates the results for the impedance spectrum on GN/GCE (a) and PNEGHNs/GCE (b) in a solution of 5 mM $Fe(CN)_6^{3-/4-}$ in 0.1 M KCl. The Randles circuit (inset of Figure 6D) was chosen to fit the impedance data obtained. It is found that PNEGHNs/GCE has a lower charge-transfer resistance value than that of GNs/GCE, demonstrating PNEGHNs have higher electrochemical activity than GNs. In addition, the electrical conductivity of PNEHNs film (1.6×10^4 S m^{-1})

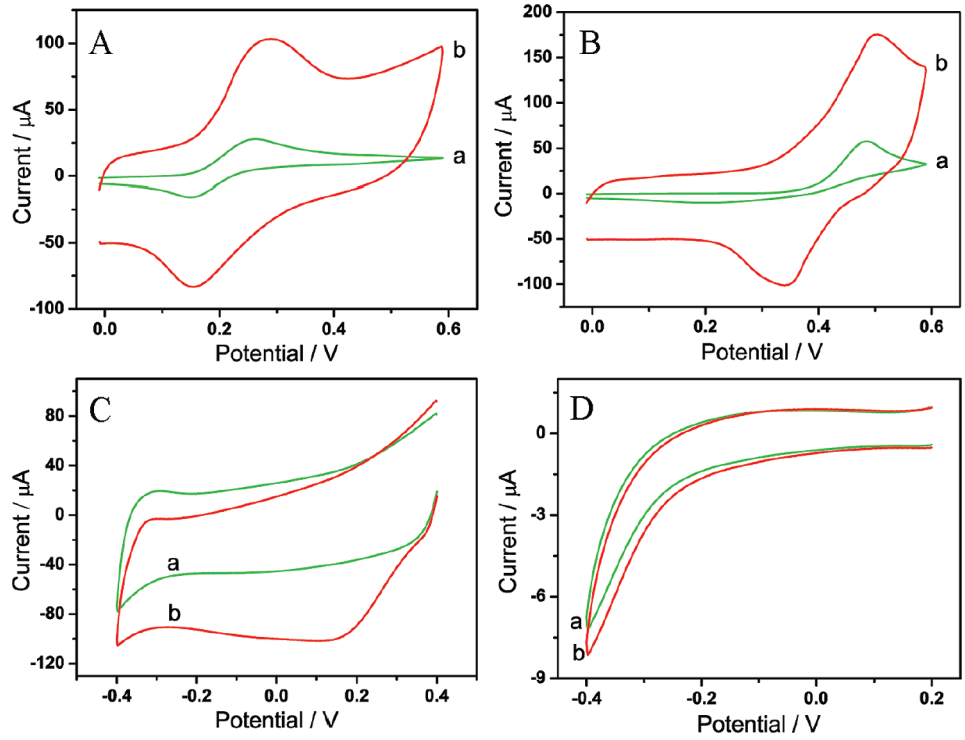

Figure 7. (A, B) CVs of DA (A) and APAP (B) on GNs/GCE (a) and PNEGHNs/GCE (b) in a PBS (pH 7.0) at the scan rate of 50 mV/s. (C, D) CVs of PNEGHNs/GCE (C) and GNs/GCE (D) in a PBS (pH 7.0) in the absence (a) and presence (b) of 2 mM H_2O_2.

measured *via* the four-point method was found to be larger than that of PMAA-functionalized GNs film (3.3×10^2 S m^{-1}), which is good accord with the above EIS result.

To further demonstrate the enhanced electrochemical performance, DA (a neurotransmitter that affects the brain processes that control movement, emotional response, and the capacity to feel pleasure and pain), APAP (one of the most extensively employed drugs in the world, a noncarcinogenic drug, and an effective substitute for aspirin), and H_2O_2 (an essential mediator in food, pharmaceutical, clinical, industrial, and environmental analyses and also an important product of oxidized-enzymes) were chosen as representative probes to study their electrochemical performance. Figure 7A,B shows the electrochemical response of DA (A) and APAP (B) on the GNs/GCE (a) and PNEGHNs/GCE (b) in 0.1 M PBS (pH 7.0) containing 1 mM DA and 2.5 mM APAP, respectively. The oxidation peak currents of two compounds are increased at PNEGHNs/GCE relative to GN/GCE, indicating a favorable catalytic activity of PNEGHNs toward the oxidation of two compounds. Figure 7C,D shows the CVs of PNEGHNs/GCE (C) and GNs/GCE (D) in the absence (a) and presence (b) of 2 mM H_2O_2 in 0.1 M PBS (pH 7.0). Much higher current and lower overpotential are found on PNEGHNs/GCE than that of GNs/GCE, which further reveal that PNEGHNs are excellent materials for electrochemical sensing.

To test the electrochemical sensing ability of PNEGHNs, H_2O_2 was chosen as one of the target analytes. Figure 8A compares the amperometric responses of different electrodes with successive additions of H_2O_2. Compared with GNs/GCE (a), as H_2O_2 was added to the stirring buffer solution, PNEGHNs/GCE (b) responded rapidly to the substrate and achieved steady-state current within 4 s. A good linear relationship (Figure 8B) was realized between the reduction peak current of H_2O_2 and its concentration in the range of 1 μM to 500 μM, with the detection limit of 80 nM based on $S/N = 3$. It is worthwhile noting that the detection limit of H_2O_2 at the PNEGHNs/GC electrode is lower than those at carbon materials-based modified electrodes, such as the CNTs/chitosan modified electrode (10.3 μM),[51] the CNTs paste electrode (60 μM),[52] the highly ordered mesoporous carbon modified electrode (1.61 μM),[53] the platelet-carbon nanofibers modified electrode (4.0 μM),[54] CNTs/silica/Au/Pt hybrid nanomaterial (0.5 μM),[55] gold nanowire assembling sphere (1.2 μM),[56] mesoporous Pt (4.5 μM),[57] graphene/Au NPs/chitosan (180 μM)[58] and certain horse radish peroxidase (HRP)-based biosensors (*e.g.*, 12.89 μM for sol−gel derived ceramic-CNT-HRP nanocomposite; 1.7 μM for Au-graphene-HRP-chitosan biocomposite),[59−61] *etc.*, indicating that PNEGHNs are an excellent choice for the enhanced electrochemical sensing. Moreover, PNEGHNs/GCE shows a very high selectivity for the detection of H_2O_2; 0.1 mM of AA and UA in 0.1 M PBS (pH 7.0) did not show interferences to 0.05 mM H_2O_2 detection, indicating its high selectivity toward H_2O_2 detection, as shown in Figure 8C. The PNEGHNs-based H_2O_2 sensor also exhibits a good long-term

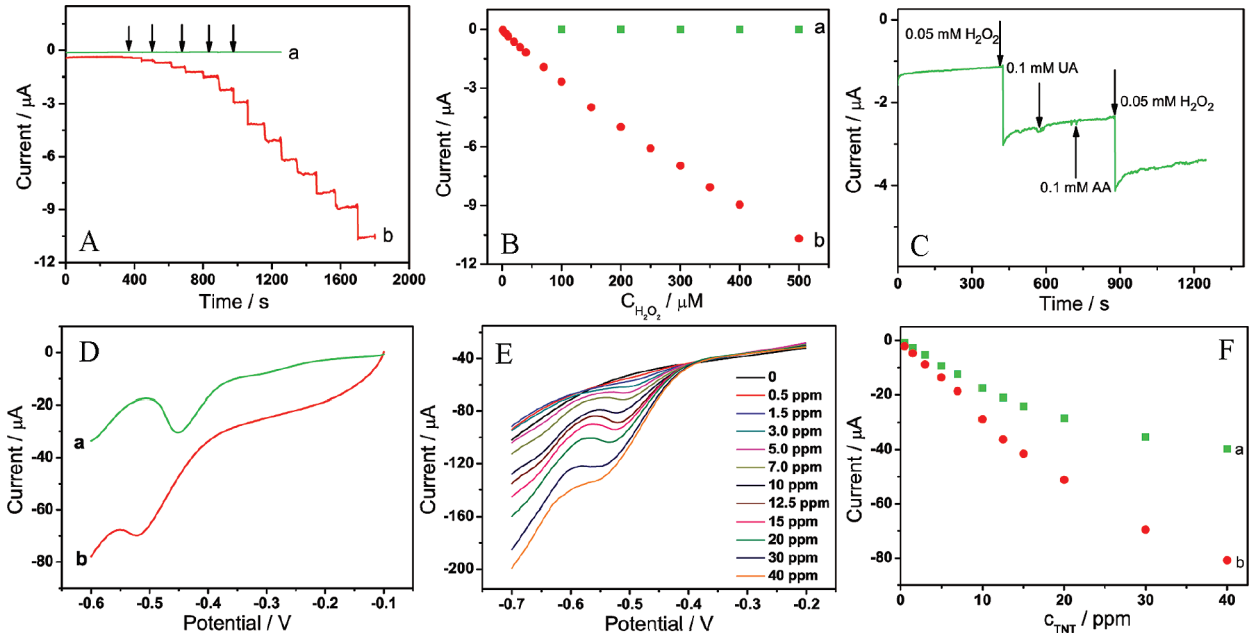

Figure 8. (A) Current−time recordings for successive additions of H_2O_2 at the GNs/GCE (a) and PNEGHNs/GCE (b) measured at 0 V. (B) The plot of current of H_2O_2 *versus* its concentrations. (C) Current responses of the PNEGHNs/GCE to the sequential additions of 0.05 mM H_2O_2, 0.1 mM AA, and 0.1 mM UA into 0.1 M PBS. (D) ASV curves of GNs/GCE (a) and PNEGHNs/GCE (b) in a PBS (pH 9.4) in the presence of 10 ppm TNT at the scan rate of 50 mV/s. (E) ASV curve of PNEGHNs/GCE in a PBS (pH 9.4) in the presence of TNT with different concentrations at the scan rate of 50 mV/s. (F) The plot of currents of TNT *versus* its concentrations obtained at GNs/GCE (a) and PNEGHNs/GCE (b).

stability. The catalytic current response can maintain over 90% of its initial value even after one month.

On the other hand, the study of trinitrotoluene (TNT), a typical explosive compound, has attracted considerable attention from chemists owing to its importance in environmental protection and antiterrorism.[62] It is therefore imperative to develop new protocols to detect and analyze TNT. Electrochemical techniques have been proved useful for detecting TNT due to their high sensitivity and simplicity, and it is easy to fabricate inexpensive and portable detectors.[62] Figure 8D shows the adsorptive stripping voltammetric (ASV) curve of GNs/GCE (a) and PNEGHNs/GCE (b) in the presence of 10 ppm TNT. It is found that PNEGHNs exhibited enhanced electrochemical response toward TNT reduction relative to GNs, indicating that PNEGHNs can probably act as an enhanced electrochemical platform for detecting TNT. Figure 8E displays stripping voltammograms of PNEGHNs/GCE recorded at the different TNT concentrations over the 0.5−40 ppm range. It is observed that the peak currents on PNEGHNs/GCE increase proportionally with the TNT concentration to yield a highly linear calibration plot (Figure 8F, curve b), with a higher sensitivity than GNs/GCE (Figure 8F, line a). And the detection limit on PNEGHNs is about 0.3 ppm, which is lower than those of recent state-of-art nanomaterials such as TiO_2/Au hybrid nanostructure,[63] *etc.* Additionally, excellent reproducibility was also obtained using the same PNEGHNs/GCE for 10 repeated analyses of 3 ppm of TNT (figure not shown) resulting in a relative standard deviation of 1.9%.

CONCLUSIONS

A one-step, microwave-assisted heating reduction strategy for the rapid preparation of graphene/Pt hybrids was demonstrated. The proposed method was unique in its simplicity. The resulting PNEGHNs were used as advanced electrode materials and extensively investigated by various characterization methods, including AFM, TEM, HRTEM, XRD, XPS, and Raman spectroscopy. The new composite material combines the unique and attractive electrocatalytic behavior of GNs with good electronic and catalytic properties of Pt NPs. Particularly, we verified that a few organic and inorganic electroactive interests at PNEGHNs/GCE exhibited much higher electrochemical activity than that of GNs/GCE, suggesting the potential applications of PNEGHNs film for constructing efficient biosensing, energy-conversion, biomedical, and other electronic systems.

EXPERIMENTAL SECTION

Materials. Graphene oxide (GO) was synthesized from graphite (Afar Aster) by a modified Hummers method.[21−23] H_2PtCl_6, EG, KH_2PO_4, Na_2HPO_4, H_2SO_4, H_2O_2 (30 wt % in H_2O), DA, APAP, and TNT were obtained from Beijing Chemical Reagent Company (Beijing, China). PMAA (30 wt % in H_2O, M_w 9500) was obtained from Aldrich. Water used throughout all experiments was purified with the Millipore system; 0.1 M phosphate buffer solution (PBS) was used as a supporting electrolyte.

Apparatus. TEM and HRTEM images were obtained with a TECNAI G_2 high-resolution transmission electron microscope

operating at 200 kV. XRD analysis was carried out on a D/Max 2500 V/PC X-ray diffractometer using Cu (40 kV, 30 mA) radiation. XPS measurement was performed on an ESCALAB-MKII 250 photoelectron spectrometer (VG Co.) with Al Kα X-ray radiation as the X-ray source for excitation. Tapping-mode AFM was conducted with a SPA400 equipped with a SPI-3800 controller (Seiko Instruments Industry Co., Japan) at room temperature. Raman spectrum was recorded with a Renishaw 2000 equipped by an Ar^+ ion laser giving the excitation line of 514.5 nm and an air-cooling charge-coupled device (CCD) as the detector (Renishaw Co., U.K.). Electrochemical experiments were performed with a CHI 832 electrochemical analyzer (CH Instruments, Chenhua Co., Shanghai, China). A conventional three-electrode cell was used, including an Ag/AgCl (saturated KCl) electrode as reference electrode, a platinum wire as counter-electrode and modified GCE as working electrode. The electrochemical impedance measurements were carried out with an Autolab/PG30 electrochemical analyzer system (ECO Chemie B. V., Netherlands) in a grounded Faraday cage at ambient temperature. The interfacial charge-transfer resistances for different modified surface were determined by EIS in the frequency range between 1 Hz and 1 MHz with a perturbation signal of 5 mV.

Synthesis of PMAA-Functionalized GNs. A 5 mL portion of 1 mg/mL GO EG solution was added into 5 mL of water, followed by the addition of 1 mL of EG and 0.2 mL of PMAA. After being immediately sonicated for about 2 min, the solution was placed in the microwave oven for 90 s (power: 800 W). The product was isolated and residual PMAA was removed by centrifugation at 14000 rpm, and redispersed in water (8 mL) with sonication to produce a colloidal suspension.

Synthesis of PMAA-Protected Pt NPs. A 1 mL portion of 77 mM H_2PtCl_6 EG solution was added into the mixture containing 5 mL of EG and 5 mL of water, followed by the addition of 0.2 mL of PMAA. After being immediately sonicated for about 2 min, the solution was placed in the microwave oven for 90 s (power: 800 W). The product was dialyzed for 24 h and dispersed in 8 mL of water.

Synthesis of PNEGHNs. In a typical synthesis, 5 mL of 1 mg/mL GO EG solution was added into 5 mL of water, followed by the addition of 1 mL of 77 mM H_2PtCl_6 EG solution and 0.2 mL of PMAA. After being immediately sonicated for about 2 min, the solution was placed for microwave oven for 90 s (power: 800 W). The product was isolated and residual PMAA was removed by centrifugation at 8000 rpm for 15 min, followed by consecutive washing/centrifugation cycles three times with water. The collected product was redispersed in water/ethanol mixture (8 mL) with sonicating to produce a colloidal suspension.

Electrocatalytic Experiments. Prior to the surface coating, the GC electrode was polished carefully with 1.0, 0.3, and 0.05 μm alumina powder, respectively, and rinsed with deionized water, followed by sonication in acetone and doubly distilled water successively. Then, the electrode was allowed to dry under nitrogen. For cyclic votammetry and linear sweep voltammetry (LSV), 5 μL of PNEGHNs or PMAA-functionalized GNs or Pt NPs was dropped on the surface of GC electrode and dried with an infrared lamp. For current−time experiments, 4 μL of Nafion (0.5%) was additionally cast on the surface of the above materials-modified GC electrode and dried before electrochemical experiments. The electrochemical determination of TNT consisted of two consecutive steps: (i) preconcentration of the analytes from the stirred solution to the electrode poised at 0.0 V with an accumulation time of 100 s; (ii) reductive stripping using LSV detection at the scan rate of 50 mV/s.

Acknowledgment. This work was supported by the National Natural Science Foundation of China (No. 20820102037) and the 973 Project (Nos. 2009CB930100 and 2010CB933600). TNT was supplied by the Institute of Forensic Science, Ministry of Public Security (China), and its stock solution (3 mg/mL) was prepared in acetonitrile.

Supporting Information Available: TEM image of Pt nanoparticles. This material is available free of charge *via* the Internet at http://pubs.acs.org.

REFERENCES AND NOTES

1. Guo, S. J.; Wang, E. K. Synthesis and Electrochemical Applications of Gold Nanoparticles. *Anal. Chim. Acta* **2007**, *598*, 181–192.
2. Guo, S. J.; Dong, S. J. Biomolecule−Nanoparticle Hybrids for Electrochemical Biosensors. *Trends Anal. Chem.* **2009**, *28*, 96–109.
3. Wang, J.; Li, M.; Shi, Z.; Li, N.; Gu, Z. Direct Electrochemistry of Cytochrome *c* at a Glassy Carbon Electrode Modified with Single-Wall Carbon Nanotubes. *Anal. Chem.* **2002**, *74*, 1993–1997.
4. Kachoosangi, R. T.; Musameh, M. M.; Abu-Yousef, I.; Yousef, J. M.; Kanan, S. M.; Xiao, L.; Davies, S. G.; Russell, A.; Compton, R. G. Carbon Nanotube−Ionic Liquid Composite Sensors and Biosensors. *Anal. Chem.* **2009**, *81*, 435–442.
5. Boo, H.; Jeong, R.-A.; Park, S.; Kim, K. S.; An, K. H.; Lee, Y. H.; Han, J. H.; Kim, H. C.; Chung, T. D. Electrochemical Nanoneedle Biosensor Based on Mmultiwall Carbon Nanotube. *Anal. Chem.* **2006**, *78*, 617–620.
6. Male, K. B.; Hrapovic, S.; Santini, J. M.; Luong, J. H. T. Biosensor for Arsenite Using Arsenite Oxidase and Multiwalled Carbon Nanotube Modified Electrodes. *Anal. Chem.* **2007**, *79*, 7831–7837.
7. Zhang, M.; Liu, K.; Xiang, L.; Lin, Y.; Su, L.; Mao, L. Carbon Nanotube-Modified Carbon Fiber Microelectrodes for *in Vivo* Voltammetric Measurement of Ascorbic Acid in Rat Brain. *Anal. Chem.* **2007**, *79*, 6559–6565.
8. Luo, H.; Shi, Z.; Li, N.; Gu, Z.; Zhuang, Q. Investigation of the Electrochemical and Electrocatalytic Behavior of Single-Wall Carbon Nanotube Film on a Glassy Carbon Electrode. *Anal. Chem.* **2001**, *73*, 915–920.
9. Ali, S. R.; Ma, Y.; Parajuli, R. R.; Balogun, Y.; Lai, W. Y.-C.; He, H. A Nonoxidative Sensor Based on a Self-Doped Polyaniline/Carbon Nanotube Composite for Sensitive and Selective Detection of the Neurotransmitter Dopamine. *Anal. Chem.* **2007**, *79*, 2583–2587.
10. Profumo, A.; Fagnoni, M.; Merli, D.; Quartarone, E.; Protti, S.; Dondi, D.; Albini, A. Multiwalled Carbon Nanotube Chemically Modified Gold Electrode for Inorganic as Speciation and Bi(III) Determination. *Anal. Chem.* **2006**, *78*, 4194–4199.
11. Chen, D.; Wang, Q.; Jin, J.; Wu, P.; Wang, H.; Yu, S.; Zhang, H.; Cai, C. Low-Potential Detection of Endogenous and Physiological Uric Acid at Uricase-Thionine-Single-Walled Carbon Nanotube Modified Electrodes. *Anal. Chem.* **2010**, *82*, 2448–2455.
12. Vamvakaki, V.; Tsagaraki, K.; Chaniotakis, N. Carbon Nanofiber-Based Glucose Biosensor. *Anal. Chem.* **2006**, *78*, 5538–5542.
13. Hao, C.; Ding, L.; Zhang, X.; Ju, H. Biocompatible Conductive Architecture of Carbon Nanofiber-Doped Chitosan Prepared with Controllable Electrodeposition for Cytosensing. *Anal. Chem.* **2007**, *79*, 4442–4447.
14. Wu, L.; Zhang, X.; Ju, H. Detection of NADH and Ethanol based on Catalytic Activity of Soluble Carbon Nanofiber with Low Overpotential. *Anal. Chem.* **2007**, *79*, 4538–4542.
15. Zhou, M.; Guo, J.; Guo, L.-P.; Bai, J. Electrochemical Sensing Platform based on the Highly Ordered Mesoporous Carbon-Fullerene System. *Anal. Chem.* **2008**, *80*, 4642–4650.
16. Zhou, M.; Shang, L.; Li, B.; Huang, L.; Dong, S. Highly Ordered Mesoporous Carbons as Electrode Material for the Construction of Electrochemical Dehydrogenase- and Oxidase-Based Biosensors. *Biosens. Bioelectron.* **2008**, *24*, 442–447.
17. Zhou, M.; Ding, J.; Guo, L.-P.; Shang, Q.-K. Electrochemical Behavior of L-Cysteine and its Detection at Ordered Mesoporous Carbon-Modified Glassy Carbon Electrode. *Anal. Chem.* **2007**, *79*, 5328–5335.
18. Zhang, J.; Lei, J. P.; Xu, C. L.; Ding, L.; Ju, H. X. Carbon Nanohorn Sensitized Electrochemical Immunosensor for

Rapid Detection of Microcystin-LR. *Anal. Chem.* **2010**, *82*, 1117–1122.
19. Liu, X.; Shi, L.; Niu, W.; Li, H.; Xu, G. Amperometric Glucose Biosensor Based on Single-Walled Carbon Nanohorns. *Biosens. Bioelectron.* **2008**, *23*, 1887–1890.
20. Wen, D.; Deng, L.; Zhou, M.; Guo, S.; Shang, L.; Xu, G.; Dong, S. A Biofuel Cell with a Single-Walled Carbon Nanohorn-Based Bioanode Operating at Physiological Condition. *Biosens. Bioelectron.* **2010**, *25*, 1544–1547.
21. Guo, S.; Dong, S.; Wang, E. 21.Three-Dimensional Pt-on-Pd Bimetallic Nanodendrites Supported on Graphene Nanosheet: Facile Synthesis and Used as an Advanced Nanoelectrocatalyst for Methanol Oxidation. *ACS Nano* **2010**, *4*, 547–555.
22. Guo, H.-L.; Wang, X.-F.; Qian, Q.-Y.; Wang, F.-B.; Xia, X.-H. A Green Approach to the Synthesis of Graphene Nanosheets. *ACS Nano* **2009**, *3*, 2653–2659.
23. Stankovich, S.; Dikin, D. A.; Piner, R. D.; Kohlhaas, K. A.; Kleinhammes, A.; Jia, Y. Y.; Wu, Y.; Nguyen, S. T.; Ruoff, R. S. Synthesis of Graphene-Based Nanosheets *via* Chemical Reduction of Exfoliated Graphite Oxide. *Carbon* **2007**, *45*, 1558–1565.
24. Lee, C.; Wei, X.; Kysar, J. W.; Hone, J. Measurement of the Elastic Properties and Intrinsic Strength of Monolayer Graphene. *Science* **2008**, *321*, 385–388.
25. Xia, F.; Mueller, T.; Lin, Y.; Valdes-Garcia, A.; Avouris, P. Ultrafast Graphene Photodetector. *Nat. Nanotechnol.* **2009**, *4*, 839–843.
26. Li, X. L.; Wang, X. R.; Zhang, L.; Lee, S.; Dai, H. J. Chemically Derived, Ultrasmooth Graphene Nanoribbon Semiconductors. *Science* **2008**, *319*, 1229–1232.
27. Pang, S. P.; Tsao, H. N.; Feng, X. L.; Müllen, K. Patterned Graphene Electrodes from Solution-Processed Graphite Oxide Films for Organic Field-Effect Transistors. *Adv. Mater.* **2009**, *21*, 3488–3491.
28. Wu, Z.-S.; Pei, S. F.; Ren, W. C.; Tang, D. M.; Gao, L. B.; Liu, B. L.; Li, F.; Liu, C.; Cheng, H.-M. Field Emission of Single-Layer Graphene Films Prepared by Electrophoretic Deposition. *Adv. Mater.* **2009**, *21*, 1756–1760.
29. Xu, Y. F.; Liu, Z. B.; Zhang, X. L.; Wang, Y.; Tian, J. G.; Huang, Y.; Ma, Y. F.; Zhang, X. Y.; Chen, Y. S. A Graphene Hybrid Material Covalently Functionalized with Porphyrin: Synthesis and Optical Limiting Property. *Adv. Mater.* **2009**, *21*, 1275–1279.
30. Watcharotone, S.; Dikin, D. A.; Stankovich, S.; Piner, R.; Jung, I.; Dommett, G. H. B.; Evmenenko, G.; Wu, S.-E.; Chen, S.-F.; Liu, C.-P.; *et al*. Graphene-Silica Composite Thin Films as Transparent Conductors. *Nano Lett.* **2007**, *7*, 1888–1892.
31. Vickery, J. L.; Patil, A. J.; Mann, S. Fabrication of Graphene−Polymer Nanocomposites with Higher-Order Three-Dimensional Architectures. *Adv. Mater.* **2009**, *21*, 2180–2184.
32. Seger, B.; Kamat, P. V. Electrocatalytically Active Graphene−Platinum Nanocomposites. Role of 2-D Carbon Support in PEM Fuel Cells. *J. Phys. Chem. C* **2009**, *113*, 7990–7995.
33. Wang, D. H.; Choi, D.; Li, J.; Yang, Z. G.; Nie, Z. M.; Kou, R.; Hu, D. H.; Wang, C. M.; Saraf, L. V.; Zhang, J.; *et al*. Self-Assembled TiO_2-Graphene Hybrid Nanostructures for Enhanced Li-Ion Insertion. *ACS Nano* **2009**, *3*, 907–914.
34. Zhang, K.; Zhang, L. L.; Zhao, X. S.; Wu, J. Graphene/Polyaniline Nanofiber Composites as Supercapacitor Electrodes. *Chem. Mater.* **2010**, *22*, 1392–1401.
35. Wang, X.; Zhi, L.; Müllen, K. Transparent, Conductive Graphene Electrodes for Dye-Sensitized Solar Cells. *Nano Lett.* **2008**, *8*, 323–327.
36. Tang, L. H.; Wang, Y.; Li, Y. M.; Feng, H. B.; Lu, J.; Li, J. H. Preparation, Structure, and Electrochemical Properties of Reduced Graphene Sheet Films. *Adv. Funct. Mater.* **2009**, *19*, 2782–2789.
37. Zhou, M.; Zhai, Y.; Dong, S. Electrochemical Sensing and Biosensing Platform Based on Chemically Reduced Graphene Oxide. *Anal. Chem.* **2009**, *81*, 5603–5613.
38. Shan, C.; Yang, H.; Han, D.; Zhang, Q.; Ivaska, A.; Niu, L. Electrochemical Determination of NADH and Ethanol Based on Ionic Liquid-Functionalized Graphene. *Biosens. Bioelectron.* **2010**, *25*, 1504–1508.
39. Kang, X.; Wang, J.; Wu, H.; Aksay, I. A.; Liu, J.; Lin, Y. Glucose Oxidase-Graphene-Chitosan Modified Electrode for Direct Electrochemistry and Glucose Sensing. *Biosens. Bioelectron.* **2009**, *25*, 901–905.
40. Wang, Y.; Li, Y.; Tang, L.; Lu, J.; Li, J. Application of Graphene-Modified Electrode for Selective Detection of Dopamine. *Electrochem. Commun.* **2009**, *11*, 889–892.
41. Li, Y.; Gao, W.; Ci, L.; Wang, C.; Ajayan, P. M. Catalytic Performance of Pt Nanoparticles on Reduced Graphene Oxide for Methanol Electro-oxidation. *Carbon* **2010**, *48*, 1124–1130.
42. Si, Y.; Samulski, E. T. Exfoliated Graphene Separated by Platinum Nanoparticles. *Chem. Mater.* **2008**, *20*, 6792–6797.
43. Yoo, E.; Okata, T.; Akita, T.; Kohyama, M.; Nakamura, J.; Honma, I. Enhanced Electrocatalytic Activity of Pt Subnanoclusters on Graphene Nanosheet Surface. *Nano Lett.* **2009**, *9*, 2255–2259.
44. Kou, R.; Shao, Y.; Wang, D.; Engelhard, M. H.; Kwak, J. H.; Wang, J.; Viswanathan, V. V.; Wang, C.; Lin, Y.; Wang, Y.; *et al*. *Electrochem. Commun.* **2009**, *11*, 954–957.
45. Shao, Y.; Zhang, S.; Wang, C.; Nie, Z.; Liu, J.; Wang, Y.; Lin, Y. Highly Durable Graphene Nanoplatelets Supported Pt Nanocatalysts for Oxygen Reduction. *J. Power Sources* **2010**, *195*, 4600–4605.
46. Lu, J.; Do, I.; Drzal, L. T.; Worden, R. M.; Lee, I. Nanometal-Decorated Exfoliated Graphite Nanoplatelet Based Glucose Biosensors with High Sensitivity and Fast Response. *ACS Nano* **2008**, *2*, 1825–1832.
47. Zhu, Y.-J.; Wang, W.-W.; Qi, R.-J.; Hu, X.-L. Microwave-Assisted Synthesis of Single-Crystalline Tellurium Nanorods and Nanowires in Ionic Liquids. *Angew. Chem., Int. Ed.* **2004**, *43*, 1410–1414.
48. Wang, H.; Robinson, J. T.; Li, X.; Dai, H. Solvothermal Reduction of Chemically Exfoliated Graphene Sheets. *J. Am. Chem. Soc.* **2009**, *131*, 9910–9911.
49. Bai, H.; Xu, Y.; Zhao, L.; Li, C.; Shi, G. Noncovalent Functionalization of Graphene Sheets by Sulfonated Polyaniline. *Chem. Commun.* **2009**, 1667–1669.
50. Xu, Y.; Bai, H.; Lu, G.; Li, C.; Shi, G. Flexible Graphene Films *via* the Filtration of Water-Soluble Noncovalent Functionalized Graphene Sheets. *J. Am. Chem. Soc.* **2008**, *130*, 5856–5857.
51. Qian, L.; Yang, X. Composite Film of Carbon Nanotubes and Chitosan for Preparation of Amperometric Hydrogen Peroxide Biosensor. *Talanta* **2006**, *68*, 721–727.
52. Rubianes, M. D.; Rivas, G. A. Carbon Nanotubes Paste Electrode. *Electrochem. Commun.* **2003**, *5*, 689–694.
53. Zhou, M.; Shang, L.; Li, B.; Huang, L.; Dong, S. Highly Ordered Mesoporous Carbons as Electrode Material for the Construction of Electrochemical Dehydrogenase- and Oxidase-Based Biosensors. *Biosens. Bioelectron.* **2008**, *24*, 442–447.
54. Li, Z.; Cui, X.; Zheng, J.; Wang, Q.; Lin, Y. Effects of Microstructure of Carbon Nanofibers for Amperometric Detection of Hydrogen Peroxide. *Anal. Chim. Acta* **2007**, *597*, 238–244.
55. Guo, S.; Li, J.; Ren, W.; Wen, D.; Dong, S.; Wang, E. Carbon Nanotube/Silica Coaxial Nanocable as a Three-Dimensional Support for Loading Diverse Ultra-High-Density Metal Nanostructures: Facile Preparation and Use as Enhanced Materials for Electrochemical Devices and SERS. *Chem. Mater.* **2009**, *21*, 2247–2257.
56. Guo, S.; Wen, D.; Dong, S.; Wang, E. Gold Nanowire Assembling Architecture for H_2O_2 Electrochemical Sensor. *Talanta* **2009**, *77*, 1510–1517.
57. Evans, S. A. G.; Elliott, J. M.; Andrews, L. M.; Bartlett, P. N.; Doyle, P. J.; Denuault, G. Detection of Hydrogen Peroxide at Mesoporous Platinum Microelectrodes. *Anal. Chem.* **2002**, *74*, 1322–1326.
58. Shan, C.; Yang, H.; Han, D.; Zhang, Q.; Ivaska, A.; Niu, L.

Graphene/AuNPs/Chitosan Nanocomposites Film for Glucose Biosensing. *Biosens. Bioelectron.* **2010**, *25*, 1070–1074.
59. Zhou, K.; Zhu, Y.; Yang, X.; Luo, J.; Li, C.; Luan, S. A Novel Hydrogen Peroxide Biosensor Based on Au−Graphene−HRP−Chitosan Biocomposites. *Electrochim. Acta* **2010**, *55*, 3055–3060.
60. Chen, H.; Dong, S. Direct Electrochemistry and Electrocatalysis of Horseradish Peroxidase Immobilized in Sol-Gel-Derived Ceramic-Carbon Nanotube Nanocomposite Film. *Biosens. Bioelectron.* **2007**, *22*, 1811–1815.
61. Lei, C.; Hu, S.; Gao, N.; Shen, G.; Yu, R. An Amperometric Hydrogen Peroxide Biosensor Based on Immobilizing Horseradish Peroxidase to a Nano-Au Monolayer Supported by Sol−Gel Derived Carbon Ceramic Electrode. *Bioelectrochemistry* **2004**, *65*, 33–39.
62. Wen, R.; Zhang, H.-X.; Yan, C.-J.; Yan, H.-J.; Pan, G.-B.; Wan, L.-J. TNT Adsorption on Au(111): Electrochemistry and Adlayer Structure. *Chem. Commun.* **2008**, 1877–1879.
63. Filanovsky, B.; Markovsky, B.; Bourenko, T.; Perkas, N.; Persky, R.; Gedanken, A.; Aurbach, D. Carbon Electrodes Modified with TiO_2/Metal Nanoparticles and Their Application for the Detection of Trinitrotoluene. *Adv. Funct. Mater.* **2007**, *17*, 1487–1492.